A radio- and fluorescently labelled tracer for imaging and quantification of bacterial infection on orthopaedic prostheses

Welling, M.M.; Warbroek, K.; Khurshid, C.; Oosterom, M.N. van; Rietbergen, D.D.D.; Boer, M.G.J. de; ... ; Buckle, T.

BJR

INFECTION

A radio- and fluorescently labelled tracer for imaging and quantification of bacterial infection on orthopaedic prostheses

A PROOF OF PRINCIPLE STUDY

M. M. Welling,
K. Warbroek,
C. Khurshid,
M. N. van Oosterom,
D. D. D. Rietbergen,
M. G. J. de Boer,
R. G. H. H. Nelissen,
F. W. B. van Leeuwen,
B. G. Pijls,
T. Buckle

From Leiden University Medical Center, Leiden, Netherlands

Aims

Arthroplasty surgery of the knee and hip is performed in two to three million patients annually. Periprosthetic joint infections occur in 4% of these patients. Debridement, antibiotics, and implant retention (DAIR) surgery aimed at cleaning the infected prosthesis often fails, subsequently requiring invasive revision of the complete prosthetic reconstruction. Infection-specific imaging may help to guide DAIR. In this study, we evaluated a bacteria-specific hybrid tracer (^{99m}Tc-UBI$_{29-41}$-Cy5) and its ability to visualize the bacterial load on femoral implants using clinical-grade image guidance methods.

Methods

^{99m}Tc-UBI$_{29-41}$-Cy5 specificity for *Stapylococcus aureus* was assessed in vitro using fluorescence confocal imaging. Topical administration was used to highlight the location of *S. aureus* cultured on femoral prostheses using fluorescence imaging and freehand single photon emission CT (fhSPECT) scans. Gamma counting and fhSPECT were used to quantify the bacterial load and monitor cleaning with chlorhexidine. Microbiological culturing helped to relate the imaging findings with the number of (remaining) bacteria.

Results

Bacteria could be effectively stained in vitro and on prostheses, irrespective of the presence of biofilm. Infected prostheses revealed bacterial presence on the transition zone between the head and neck, and in the screw hole. Qualitative 2D fluorescence images could be complemented with quantitative 3D fhSPECT scans. Despite thorough chlorhexidine treatments, 28% to 44% of the signal remained present in the locations of the infection that were identified using imaging, which included 500 to 2,000 viable bacteria.

Conclusion

The hybrid tracer ^{99m}Tc-UBI$_{29-41}$-Cy5 allowed effective bacterial staining. Qualitative real-time fluorescence guidance could be effectively combined with nuclear imaging that enables quantitative monitoring of the effectiveness of cleaning strategies.

Cite this article: *Bone Joint Res* 2023;12(1):72–79.

Keywords: Infectious diseases, Orthopaedic surgery, Image-guided surgery, Molecular imaging, Fluorescence-guided surgery, Radioguided surgery , Debridement, antibiotics, and implant retention

Correspondence should be sent to Tessa Buckle; email: t.buckle@lumc.nl

doi: 10.1302/2046-3758.121.BJR-2022-0216.R1

Bone Joint Res 2023;12(1):72–79.

Article summary

Article focus

- Infection-specific image guidance may help to improve efficacy of debridement, antibiotics, and implant retention surgery.
- Hybrid bacteria-specific tracers facilitate visualization and quantification of the bacterial load on hip prosthesis.

Key messages

- The hybrid tracer ^{99m}Tc-UBI$_{29-41}$-Cy5 effectively stains bacteria.
- Topical application on femur prostheses allows identification and monitoring of bacterial infections.
- Qualitative real-time fluorescence guidance combined with nuclear imaging allowed response monitoring of bacterial cleaning approaches.

Strengths and limitations

- The hybrid nature of ^{99m}Tc-UBI$_{29-41}$-Cy5 helps to provide a direct correlation between the fluorescence and nuclear readouts for bacterial load.
- The use of clinical-grade prosthesis and imaging modalities adds to the translational potential of the imaging technology.
- The clinical potential of image guidance concepts in combination with ^{99m}Tc-UBI$_{29-41}$-Cy5 still needs to be validated in clinical trials.

Introduction

Surgical implantation of prosthesis, including hip or knee arthroplasties after osteoarthritis, and fixation of bone fractures and tendon reconstructions, are standard orthopaedic interventions. Implantation-related infections occur in 4% of knee and hip arthroplasty cases, converting to 104,000 patients/year in Europe alone.[1] Herein *Staphylococcus aureus* is the most prevalent source of infection.[2,3]

If periprosthetic joint infection (PJI) is suspected, the standard treatment modality is debridement, antibiotics, and implant retention (DAIR). Unfortunately, the reported success rates of debridement with prosthesis retention and long-term antibiotic use are found to be variable (21% to 89%).[4-8] The alternative is revision surgery, which has severe implications for the patient including prolonged hospitalization, high health and social costs,[9,10] and up to 10% risk of recurrence.[3] The latter is likely related to residual bacteria in the wound.

A number of imaging tracers for bacterial imaging have been reported in literature, including antibiotics and antimicrobial peptides.[11-16] Imaging experiments conducted with the antimicrobial peptide UBI$_{29-41}$ have demonstrated promising results in various disease models and patients. In contrast to intravenous tracer administration, topical tracer application could allow effective 'illumination' of the infection with a minimal amount of tracer.

Radiotracers have proven their value in preoperative and intraoperative imaging, whereby they allow visualization of disease using nuclear medicine imaging (e.g. single photon emission CT (SPECT) imaging) and intraoperative guidance using for example a gamma probe, both based on the radioactive signature of the tracer. Radiotracers also provide the gold standard for the quantification of pharmacokinetics based on gamma counting.[17] In parallel, fluorescent tracers are increasingly applied for image guidance,[18] allowing real-time illumination of highlighted tissue based on tracer uptake and subsequent fluorescence imaging. The synergy between nuclear and fluorescence imaging, via the use of bimodal or rather hybrid tracers, has helped to provide a best-of-both-worlds strategy in image-guided surgery.[19,20] This is achieved by facilitating both radio and fluorescence guidance with a single imaging agent. Earlier studies in rodent infection models have suggested that such a hybrid strategy could also hold promise in bacterial imaging.[18,21]

In this study, we investigated if topical application of the hybrid tracer ^{99m}Tc-UBI$_{29-41}$-Cy5 allows identification and monitoring of bacterial infections on real-size femur prostheses (Figure 1). Following compound synthesis, the tracer's capacity was microscopically studied in a mature (3D) bacterial culture that includes biofilm. The presence of bacterial infection on different regions of infected femoral stem including heads and acetabular components, as well as the impact of debridement, were macroscopically assessed using clinical-grade fluorescence and radio guidance methods.

Methods

Details on general chemistry, synthesis of UBI$_{29-41}$-Cy5-QAmine (Supplementary Figure a), compound analysis (Supplementary Figure b), radiolabelling of UBI$_{29-41}$-Cy5, and staining of bacteria and bacterial biofilm are provided in the Supplementary Material.

Culturing of bacteria and bacterial biofilm matrix. Stocks of *Staphylococcus aureus* bacteria (*S. aureus* ATCC 29213, a biofilm forming clinical isolate with a well-defined capacity of developing biofilms in vitro and in vivo; American Type Culture Collection (ATCC), USA) (stored at -20°C) containing approximately 3 × 10^9 colony-forming units (CFUs) were washed twice in 25 mM ammonium acetate buffer (pH 5).

For microscopic 3D assessment of bacterial culture, *S. aureus* was cultured in 35 mm culture dishes containing a glass insert (MatTek, USA) containing a nanofibre polystyrene cell culture scaffold (Biotek 3D Insert PS scaffold; MilliporeSigma, Netherlands). Scaffolds were incubated for four to five days at room temperature in 2 ml of brain heart infusion (BHI) broth (MilliporeSigma), containing 0.75 × 10^9 CFUs of *S. aureus*. Hereafter, scaffolds were gently washed with 2 × 2 ml of 25 mM ammonium acetate buffer pH 5. The latter is in agreement with the pH of bacterial infection and provides optimal conditions for tracer binding to the bacteria.

For macroscopic assessment of bacterial culture, eight human femoral implants (both cemented and uncemented femoral stems, of various brands; deemed unsuitable during surgical fitting, discarded, and set aside for research purposes) were used. Prior to use, the prostheses were thoroughly cleaned with bleach (5% w/v) and sterilized for 20 minutes at 120°C. Hereafter the prostheses were submerged (five to six days at room temperature) in 250 ml of 30% BHI medium in sterile PBS containing 3 × 10^9 CFUs of *S. aureus*, to allow the growth of mature biofilm

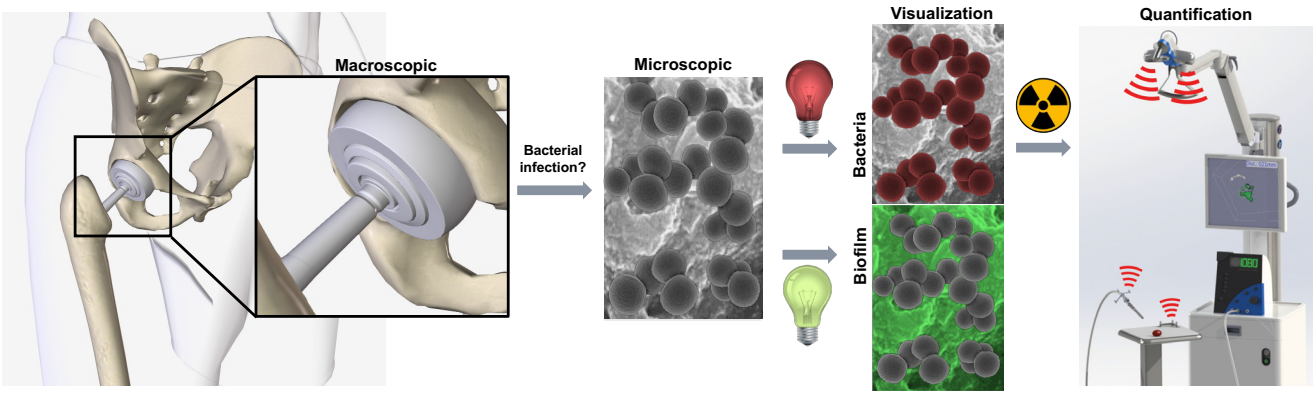

Fig. 1

Schematic overview of localization of a bacterial infection on a femoral prosthesis and experimental setup. Imaging modalities can be used to supplement macroscopic assessment of the transplanted prosthesis, thereby allowing assessment of the presence of bacterial infection based on fluorescence imaging. Visualization of the infection is achieved using fluorescence imaging. Identification of bacteria (in red) and biofilm (in green) is achieved via the use of two different tracers: ^{99m}Tc-UBI$_{29-41}$-Cy5 and SYBR Green. The hybrid nature of ^{99m}Tc-UBI$_{29-41}$-Cy5 also allows quantification of the bacterial load based on determination of radioactivity levels based on gamma counting and nuclear (single photon emission CT (SPECT)) imaging. Images were partly created using BioDigital (USA).

(standing culture). When removed from the culture, the prostheses were gently soaked twice in 25 mM ammonium acetate buffer pH 5.

Fluorescence imaging. Fluorescence confocal microscopy was performed using a Leica SP8 WLL 1 Laser Scanning Confocal Microscope (Leica Microsystems, Germany) using a 100× magnification/1.4 Oil DIC III immersion objective. Sequential scanning settings were used to visualize the different fluorescent features: Hoechst (λ_{ex} 405 nm, λ_{em} 430 to 480 nm), Cy5 (λ_{ex} = 633 nm, λ_{em} = 650 to 700 nm), and SYBR Green (λ_{ex} = 488 nm, λ_{em}= 500 to 550 nm). Fibres, bacteria, and the associated biofilm matrix images were merged and processed using LASX software (Leica Application Software Suite 4.8; Leica Microsystems) (3D via z-stack measurements and 3D reconstructions).

Macroscopic fluorescence imaging was performed using a clinical-grade fluorescence laparoscopy setup (KARL STORZ Endoskope, Germany) consisting out of a prototype modified IMAGE 1S light source with integrated Cy5 filter and matching 0° modified laparoscope (Cy5 imaging of the bacterial infection), an Image 1 HUB HD+ D-light P system (AF settings for visualization of biofilm) and a standard clinical grade 30 0° fluorescence laparoscope (HopkinsII 10mm laparoscope, Karl Storz Endoskope, Germany). Images were recorded using integrated Karl Storz software. Previously described image processing software (in-house developed and written in MATLAB (The MathWorks, USA)[22]) was adapted to allow representation of both Cy5 and SYMR Green in rainbow and heat-mapped colour-coding, respectively, which represented signal-to-background ratios (SBRs). Staining of non-infected prostheses served as controls.

Freehand SPECT imaging. A handheld gamma camera (Crystal Cam; Crystal Photonics, Germany) coupled to the Declipse SPECT (SurgicEye, Germany) was used to visualize and quantify the radioactive signature used in 2D gamma images (acquisition time: 10 s), as well as acquire 3D freehand SPECT (fhSPECT) scans (acquisition time: 3 to 5 mins).[23] Staining of non-infected prostheses served as controls. Radioactivity present on the prosthesis was counted using a dose calibrator (VDC101; Veenstra Instruments, Netherlands).

Effect of cleaning on the presence of bacterial infection. Following initial macroscopic imaging and quantitative analysis, prostheses stained with ^{99m}Tc-UBI$_{29-41}$-Cy5 were thoroughly scrubbed for two minutes with chlorhexidine (0.5% w/v chlorhexidine digluconate in ethanol 70% v/v; Added Pharma, Oss, Netherlands)[24] and washed with sterile saline. Subsequential fluorescence imaging and quantification of the radioactive signal were performed as described above. To assess the remaining viable bacteria prior to and after cleaning, sterile cotton swabs were swiped for two minutes over areas containing bacteria. Swabs were submerged in 2 ml of BHI medium in sterile test tubes, covered, and gently shaken for 17 hours at 37°C. Hereafter, the optical density (OD) of the inoculated BHI medium was measured in a Shimadzu UV-1289 Spectro-photometer (Shimadzu Benelux, Netherlands) at 600 nm (OD^{600nm}). Values were compared to the read-out of a calibration curve of OD^{600nm} values with predetermined values of viable *S. aureus* of the same strain (y = 0.033Ln(x) + 1,4618, R_2 = 0.908; see Supplementary Material for additional details and Supplementary Figure b).

Statistical analysis. All data are presented as mean values (standard deviation). The differences in radioactive counts on prostheses and various parts thereof were determined and presented with their 95% confidence intervals. Means, medians, and interquartile ranges (IQRs) were reported for quantification of the bacterial infection levels on specific locations of the prosthesis. Differences in radioactive counts and the bacterial load on prostheses and various parts were analyzed using the two-tailed independent-samples *t*-test. Statistical analysis was performed using R software version 3.6.3

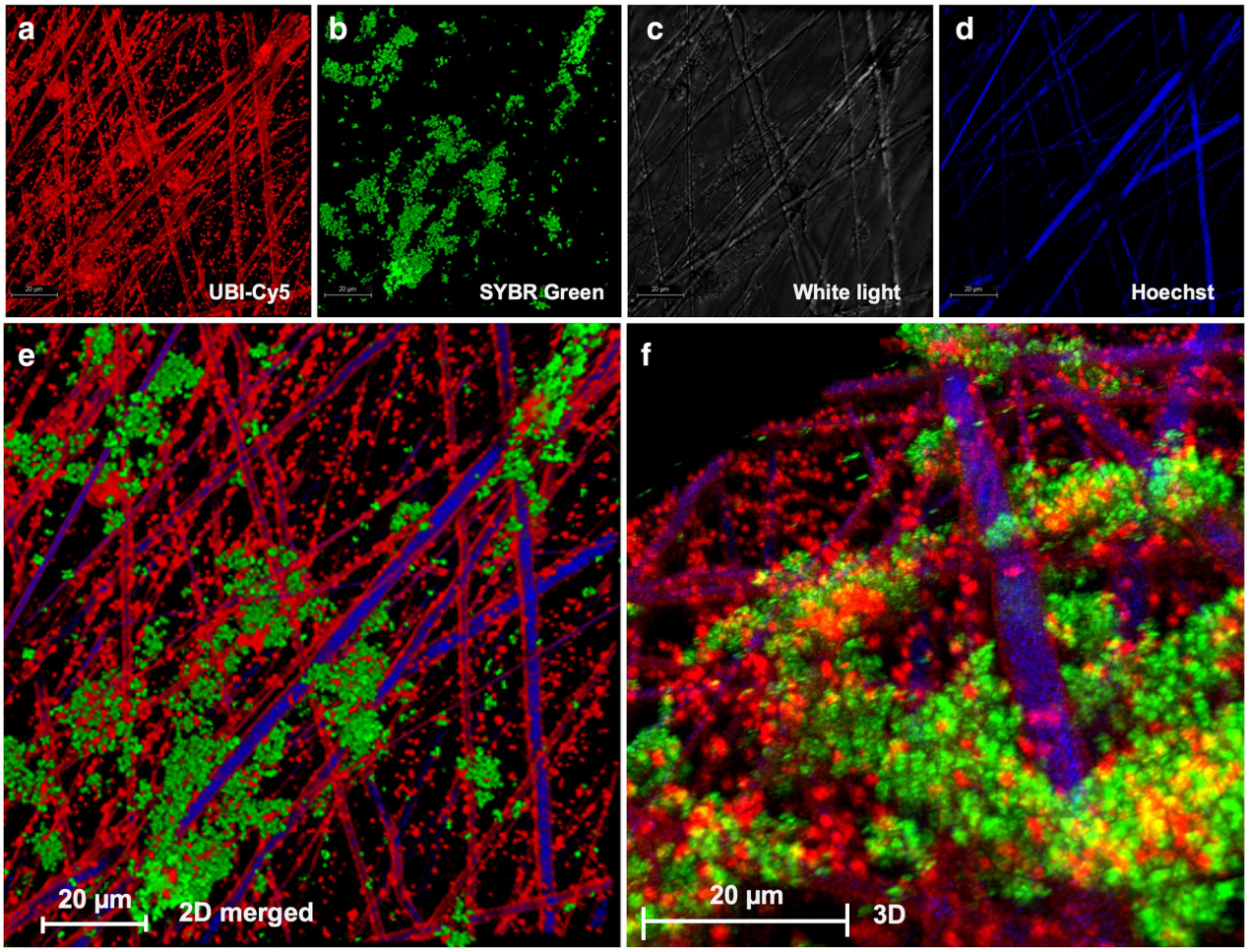

Fig. 2

Fluorescence confocal microscopy images of scaffolds containing bacteria in an associated biofilm matrix. a) *Stapylococcus aureus* is stained with UBI_{29-41}-Cy5 (red) and b) biofilm-associated matrix is stained with SYBR Green. c) The 2D white light image of scaffold fibres and scaffold fibres stained with d) Hoechst (blue). A merged image is shown in e), and a 3D image is shown in f).

(R Foundation for Statistical Computing, Austria), and all tests were two-sided with significance level set at $p < 0.05$.

Results

Microscopic visualization of bacteria and biofilm matrix. Bacterial staining was shown to be effective even in the presence of biofilm-associated matrix (bacteria in red (UBI_{29-41}-Cy5; Figure 2a) and biofilm in green (SYBR Green; Figure 2b)). Next to white light imaging (Figure 2c), nuclear Hoechst staining effectively highlight the fibres of the culture scaffold (Figure 2d, in blue).

Macroscopic fluorescence imaging of bacteria cultures on femoral stem and head prostheses. Topical application of UBI_{29-41}-Cy5 on femoral stem/head of infected prostheses revealed clear focal fluorescence staining (Figure 3, Supplementary Figure d). The highest signal intensities were measured at the junction of the femoral stem and taper (for attachment of the femoral head; Figures 3a and 3d), the rim of the femoral head (Figure 3b), and the screw hole on the 'shoulder' of the femoral implant that is used during surgical implantation (for this particular implant; Figure 3c). In general, bacterial presence was observed on scratched areas and areas with rough surfaces and sharp angles. Pseudo-coloured image processing helped to strengthen the intensity differences in the fluorescence images (Figure 3, Supplementary Figure d). The highest SBR ratios were found on the sphere's head (max SBR 3.7) and the screw hole (max SBR 4.0). The SBR could be related to the bacterial load following microbiological culturing of swabs taken from these areas (Table I). Control experiments using non-infected prostheses showed no staining after application of UBI_{29-41}-Cy5 (Supplementary Figure e). The complementary use of UBI_{29-41}-Cy5 and SYBR Green during multicolour imaging allowed subsequent visualization of bacteria and biofilm within the same image (Figure 4).

Quantitative imaging of bacterial infection. Bacterial staining with ^{99m}Tc-UBI_{29-41}-Cy5 allowed quantitative assessment of the tracer accumulation on the femoral prosthesis. To this end, protheses were placed in a dose calibrator that provided a measure of the overall activity

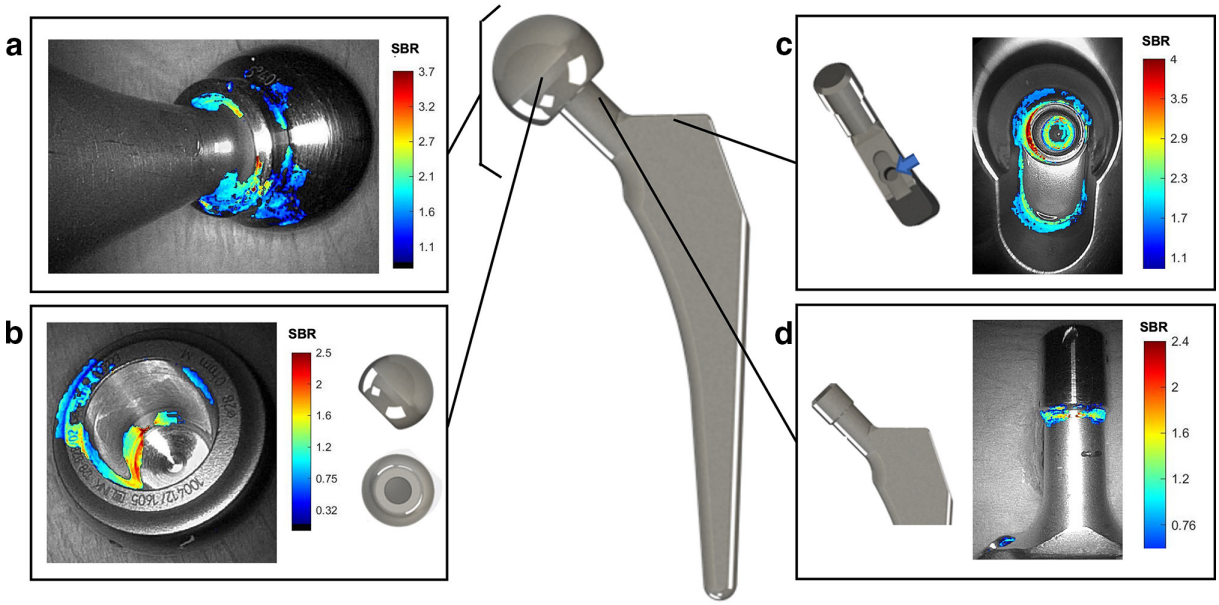

Fig. 3

Visualization of bacterial infection on a femoral prothesis. Representative pseudo-coloured fluorescence imaging of *Stapylococcus aureus* with UBI_{29-41}-Cy5 of bacterial growth on various locations on femur prosthetic implants: a) connected head and neck of the prosthesis; b) femoral head; c) prosthesis 'shoulder' with screw hole; and d) junction between femoral neck and taper (for femoral head fixation). SBR, signal-to-background ratio of fluorescence intensity with accompanying scale bar. n > 8.

Table I. Quantifying the bacterial infection.

Part of prosthesis	^{99m}Tc-UBI_{29-41} Cy5 (counts)		Viable bacteria, CFUs		p-value comparison before and after cleaning
	Mean (SD)	Median (IQR)	Mean (SD)	Median (IQR)	
Femoral sphere	1,401 (985)*	1,297 (660 to 2,108)	1.3 (1.3 × 10^7)	1.2 × 10^7 (0.1 to 2.6 × 10^7)	0.028
After cleaning	350 (189)	220 (127 to 444)	0	0 (0 to 1.8)	
Femoral neck	2,851 (2,308)*	2,666 (1,789 to 4,081)	3.5 (5.7 × 10^7)	9.4 × 10^6 (0.4 to 9.4 × 10^7)	0.025
After cleaning	616 (381)	481 (163 to 776)	0	0 (0 to 0.8)	
Screw hole	4,455 (2,305)*	4,501 (2,910 to 7,788)	1.0 (0.9 × 10^8)	2.4 × 10^7 (0.2 to 1.4 × 10^8)	0.025
After cleaning	1,842 (809)	2,272 (1,463 to 2,676)	1.1 (1.9 × 10^4)	1.6 × 10^3 (0.002 to 2 × 10^4)	

n = 8 for each parameter.
*p < 0.05 compared to radioactivity binding on cleaned prostheses.
CFU, colony-forming unit; IQR, interquartile range; SD, standard deviation.

present on the prosthesis (gamma counts; Table I). 3D fhSPECT and 2D gamma camera images were created using a handheld gamma camera (Figure 5a). Planar 2D images showed the radioactive signal in an intensity-related colour scaling, whereas fhSPECT allowed depiction of the radioactive signal in 3D via assessment under various angles. Using the Declipse SPECT, an image of the prosthesis and the radioactivity data were converted into augmented reality overlays that depicted the exact location of the radioactive signal on the prosthesis. This could be directly related to the location of the fluorescence signal on the same prosthesis (Figures 5b and 5c). Control experiments with $^{99m}TcO_4^-$ and the application of ^{99m}Tc-UBI_{29-41}-Cy5 on non-infected prostheses yielded significantly lower readouts (p = 0.039; Figures 5d and 5e).

Comparison between presence of radioactivity and the number of bacteria present on a particular site of the prosthesis allowed quantified assessment of the level of infection present in a particular area of the prosthesis (p = 0.028; Table I, Figure 5). In agreement with the SBR found for fluorescence imaging, the lowest level of infection

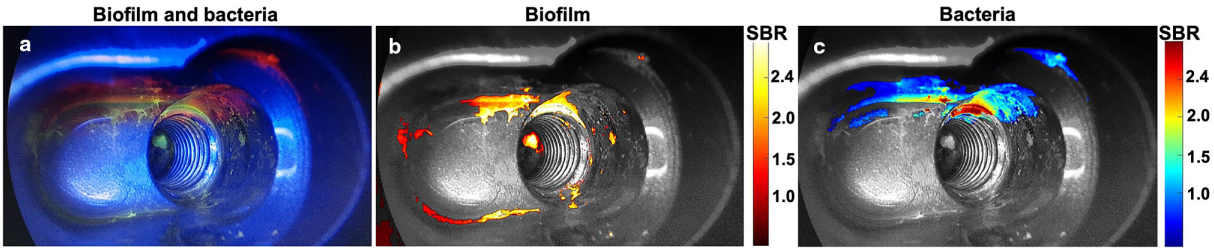

Fig. 4

Multicolour imaging of components of bacterial growth on the screw hole of a femur prosthesis. Representative imaging of: a) the biofilm unprocessed; b) at the SYBR Green filter setting and pseudo-coloured processing with SYBR Green; and c) UBI_{29-41}-Cy5. Heat bars: SBR, signal-to-background ratio of fluorescence intensity. n = 3.

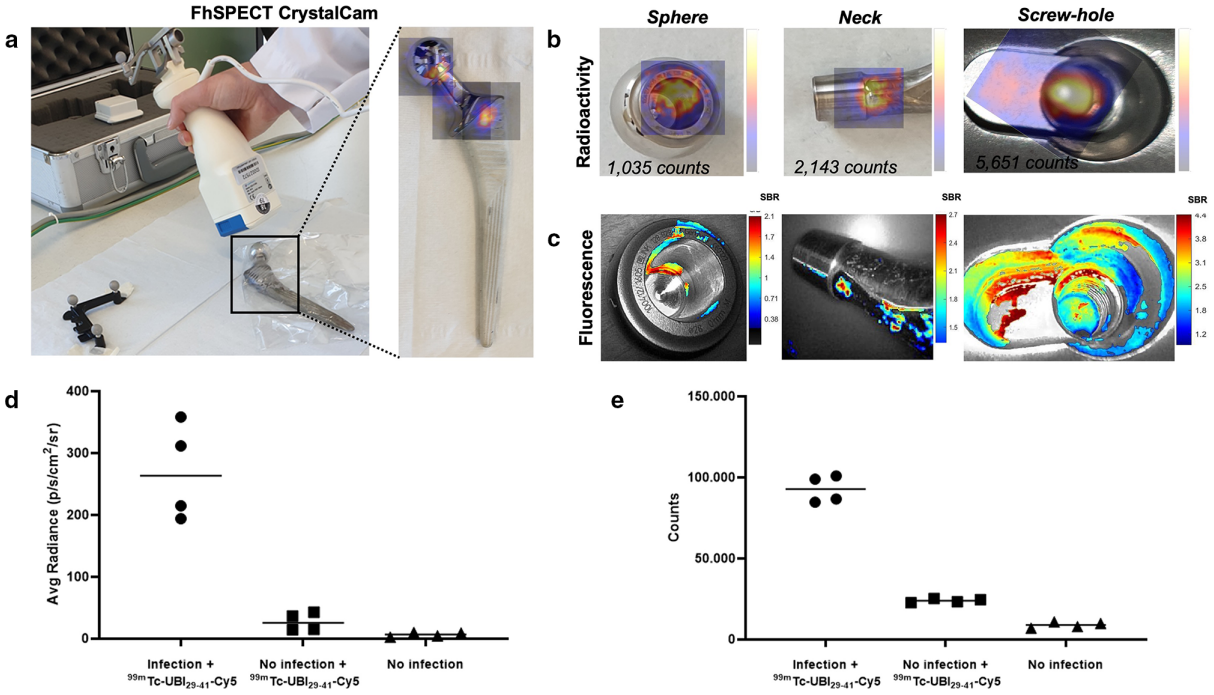

Fig. 5

Visualization of bacterial infection using ^{99m}Tc-UBI_{29-41}-Cy5. Gamma imaging allowed a) assessment of the presence and location of the bacterial infection on the femur prosthesis and b) quantification of the level of bacterial infection based on gamma counting. c) Fluorescence imaging of the corresponding locations of bacterial infection with the bacterial load represented based on the colour-coded signal-to-background ratio (SBR). d) Semiquantitative assessment of fluorescence and e) quantification of the level of radioactivity on infected prosthesis stained with ^{99m}Tc-UBI_{29-41}-Cy5 (circle), non-infected prosthesis stained with ^{99m}Tc-UBI_{29-41}-Cy5 (square), and non-infected non-stained prosthesis (triangle). fhSPECT, freehand SPECT.

was seen in the inner part of the sphere with higher levels of infection in the prosthesis neck and screw hole.

Effect of cleaning on the presence of bacterial infection. To assess the effect of cleaning of the prosthesis with chlorhexidine, radioactive counts and the mean number of viable bacteria (CFUs) were compared before and after cleaning of the areas where bacterial infection was shown on imaging (Table I). Following cleaning, the number of radioactive counts decreased by 72% and 70% for the sphere and neck, respectively (Table I), corresponding to a 7.55-log and 7.11-log reduction in remaining CFUs. However, bacterial culturing could not identify viable bacteria. As such, it appears that non-viable bacteria can remain in place after cleaning. In the screw hole, which has a rougher surface and is harder to clean, a mere 50% decrease in the number of radioactive counts and 6.84-log reduction of remaining CFUs were observed, and viable bacteria were detected (Table I).

Gamma counting and fhSPECT imaging after cleaning showed a clear decrease but not a complete disappearance of signal (Table I; Supplementary Figure vi). The relatively low detection sensitivity of fluorescence imaging hampered effective monitoring of the debridement procedure. In particular, low bacterial loads could not be accurately visualized using fluorescence imaging.

Discussion

Our findings demonstrate the feasibility of using ^{99m}Tc-UBI$_{29-41}$-Cy5 for the visualization of bacteria in both a microscopic and macroscopic manner. The use of femur protheses as a model system helped to establish critical locations for bacterial growth, and provided a setup to monitor the effectiveness of surgical debridement procedures. The fact that this could be achieved with clinical-grade methods, e.g. (multicolour) fluorescence, portable gamma camera, and fhSPECT,[22,23] indicates promise for future translation of the presented concepts into orthopaedic care. That said, further studies are needed to validate the clinical potential of presented concepts. Such studies may use infected surgical explants[25] or large animal infection models,[26] but will preferably evaluate in-human use.

Where initial visualization of bacterial infections guides DAIR, secondary imaging provides a means to monitor the response to debridement. This combination of intraoperative feedback has the potential to improve the DAIR procedure. In turn, this converts to lower non-curing rates. Novel DAIR strategies that are currently under evaluation, e.g. non-contact induction heating,[27,28] or bacteriophage-based debridement,[29] can benefit from the presented imaging paradigm both during product development and during clinical implementation.

In addition to improving the effectiveness of the DAIR procedure, bacterial imaging helps to increase the fundamental knowledge of bacterial colonization in relation to the morphology of the implant. For example, bacteria in the screw hole on the 'shoulder' of the femoral implant, which is used for implant insertion, proves particularly problematic (Figures 2c, 4, and 5), especially as these bacteria show a high persistence after therapy (Table I). This is a finding that may impact future implant designs.

Although fluorescence imaging provides a qualitative read-out, it is subject to signal attenuation and has limited sensitivity.[20] In line with this, we found that fluorescence is not the ideal modality to identify residual bacterial loads (e.g. dead or viable bacteria). As a result of our hybrid tracer design, the ^{99m}Tc radiolabel complements fluorescence imaging by providing sensitive and quantitative interpretation that allows treatment monitoring.

Translating image guidance technologies to in-human use is a costly and challenging process. This is especially the case when the imaging technologies merely enable execution of an existing treatment method such as DAIR. One could state that a new technology should help to advance care and, at the same time, its use should make sense from an economic perspective. Currently, the physical and emotional effects of PJI result in quality-adjusted life years (QALYs) of 4.4 QALYs per patient.[30,31] Valued at €40,000 per QALY, improvement in QALY outcome related to reduction of the number of repeat surgeries is already worth approximately €176,000 per patient. As such, it seems that a solid business case can be made for intraoperative bacterial imaging. This is further substantiated by the fact that the imaging methods required for the detection of ^{99m}Tc-UBI$_{29-41}$-Cy5 are already clinically available (Figures 3 and 4), and that the UBI$_{29-41}$ peptide is effective in targeting a wide variety of bacterial strains.[32–35] The fact that bacterial staining can be achieved following a topical tracer application of 40.4 ng of UBI$_{29-42}$ suggests that staining can be achieved within a micro-dosing regimen;[36,37] micro-dosing helps to limit the costs of both translation and routine implementation.

In conclusion, topical application of the hybrid bacterial tracer ^{99m}Tc-UBI$_{29-41}$-Cy5 allows bacterial visualization, therapy guidance, and quantification of debridement effectiveness on femoral implants.

Supplementary material

Supplementary methods, including general chemistry, synthesis of UBI29-41-Cy5-QAmine (UBI29-41-Cy5), radiolabelling of UBI29-41-Cy5, staining of bacteria and the bacterial biofilm, and calibration curve *Staphylococcus aureus*. Supplementary results, including HPLC and MALDI-TOF analysis of UBI29-41-Cy5-QAmine. Figures showing the molecular structure of UBI$_{29-41}$-Cy5, calibration curve for *Staphylococcus aureus* in brain heart infusion medium, analysis of UBI29-41-Cy5-QAmine, fluorescence imaging of bacterial infection on femoral prostheses, imaging of biofilm associated matrix on femur prosthesis, and effect of cleaning on the presence of bacterial infections.

References

1. **No authors listed**. Health at a Glance 2021: OECD Indicators. Hip and knee replacement. OECD iLibrary. 2022. https://www.oecd-ilibrary.org/sites/8b492d7a-en/index.html?itemId=/content/component/8b492d7a-en (date last accessed 17 November 2022).
2. **Wildeman P**, **Tevell S**, **Eriksson C**, **Lagos AC**, **Söderquist B**, **Stenmark B**. Genomic characterization and outcome of prosthetic joint infections caused by Staphylococcus aureus. *Sci Rep*. 2020;10(1):5938.
3. **Scheper H**, **van Hooven D**, **van de Sande M**, **et al**. Outcome of acute staphylococcal prosthetic joint infection treated with debridement, implant retention and antimicrobial treatment with short duration of rifampicin. *J Infect*. 2018;76(5):498–500.
4. **Kim JH**, **Chun SK**, **Yoon YC**, **Lakhotia D**, **Shon WY**. Efficacy of debridement for early periprosthetic joint infection after hip arthroplasty. *Hip Pelvis*. 2014;26(4):227–234.
5. **Craxford S**, **Marson BA**, **Nightingale J**, **et al**. Deep infection after hip hemiarthroplasty: risk factors for infection and outcome of treatments. *Bone Jt Open*. 2021;2(11):958–965.
6. **Gerritsen M**, **Khawar A**, **Scheper H**, **et al**. Modular component exchange and outcome of DAIR for hip and knee periprosthetic joint infection: a systematic review and meta-regression analysis. *Bone Jt Open*. 2021;2(10):806–812.
7. **Kildow BJ**, **Patel SP**, **Otero JE**, **et al**. Results of debridement, antibiotics, and implant retention for periprosthetic knee joint infection supplemented with the use of intraosseous antibiotics. *Bone Joint J*. 2021;103-B(6 Supple A):185–190.
8. **Morgenstern M**, **Kuehl R**, **Zalavras CG**, **et al**. The influence of duration of infection on outcome of debridement and implant retention in fracture-related infection. *Bone Joint J*. 2021;103-B(2):213–221.
9. **Berbari EF**, **Hanssen AD**, **Duffy MC**, **et al**. Risk factors for prosthetic joint infection: case-control study. *Clin Infect Dis*. 1998;27(5):1247–1254.
10. **Kapadia BH**, **McElroy MJ**, **Issa K**, **Johnson AJ**, **Bozic KJ**, **Mont MA**. The economic impact of periprosthetic infections following total knee arthroplasty at a specialized tertiary-care center. *J Arthroplasty*. 2014;29(5):929–932.

11. **Bunschoten A**, **Welling MM**, **Termaat MF**, **Sathekge M**, **van Leeuwen FWB**. Development and prospects of dedicated tracers for the molecular imaging of bacterial infections. *Bioconjug Chem*. 2013;24(12):1971–1989.
12. **Naqvi SAR**. ^{99m}Tc-labeled antibiotics for infection diagnosis: Mechanism, action, and progress. *Chem Biol Drug Des*. 2022;99(1):56–74.
13. **Ordonez AA**, **Jain SK**. Pathogen-specific bacterial imaging in nuclear medicine. *Semin Nucl Med*. 2018;48(2):182–194.
14. **Sarda-Mantel L**, **Saleh-Mghir A**, **Welling MM**, **et al**. Evaluation of 99mTc-UBI 29-41 scintigraphy for specific detection of experimental Staphylococcus aureus prosthetic joint infections. *Eur J Nucl Med Mol Imaging*. 2007;34(8):1302–1309.
15. **Schoenmakers JWA**, **Heuker M**, **López-Álvarez M**, **et al**. Image-guided in situ detection of bacterial biofilms in a human prosthetic knee infection model: a feasibility study for clinical diagnosis of prosthetic joint infections. *Eur J Nucl Med Mol Imaging*. 2021;48(3):757–767.
16. **Welling MM**, **Hensbergen AW**, **Bunschoten A**, **Velders AH**, **Roestenberg M**, **van Leeuwen FWB**. An update on radiotracer development for molecular imaging of bacterial infections. *Clin Transl Imaging*. 2019;7(2):105–124.
17. **Gemmel F**, **Van den Wyngaert H**, **Love C**, **Welling MM**, **Gemmel P**, **Palestro CJ**. Prosthetic joint infections: radionuclide state-of-the-art imaging. *Eur J Nucl Med Mol Imaging*. 2012;39(5):892–909.
18. **Welling MM**, **Hensbergen AW**, **Bunschoten A**, **et al**. Fluorescent imaging of bacterial infections and recent advances made with multimodal radiopharmaceuticals. *Clin Transl Imaging*. 2019;7(2):125–138.
19. **KleinJan GH**, **van Werkhoven E**, **van den Berg NS**, **et al**. The best of both worlds: a hybrid approach for optimal pre- and intraoperative identification of sentinel lymph nodes. *Eur J Nucl Med Mol Imaging*. 2018;45(11):1915–1925.
20. **van Leeuwen FWB**, **Schottelius M**, **Brouwer OR**, **et al**. Trending: Radioactive and fluorescent bimodal/hybrid tracers as multiplexing solutions for surgical guidance. *J Nucl Med*. 2020;61(1):13–19.
21. **Welling MM**, **de Korne CM**, **Spa SJ**, **et al**. Multimodal tracking of controlled *Staphylococcus aureus* infections in mice. *ACS Infect Dis*. 2019;5(7):1160–1168.
22. **Buckle T**, **van Alphen M**, **van Oosterom MN**, **et al**. Translation of c-met targeted image-guided surgery solutions in oral cavity cancer - initial proof of concept data. *Cancers (Basel)*. 2021;13(11):2674.
23. **Engelen T**, **Winkel BM**, **Rietbergen DD**, **et al**. The next evolution in radioguided surgery: breast cancer related sentinel node localization using a freehandSPECT-mobile gamma camera combination. *Am J Nucl Med Mol Imaging*. 2015;5(3):233–245.
24. **Pijls BG**, **Sanders IMJG**, **Kuijper EJ**, **Nelissen RGHH**. Synergy between induction heating, antibiotics, and *N*-acetylcysteine eradicates *Staphylococcus aureus* from biofilm. *Int J Hyperthermia*. 2020;37(1):130–136.
25. **van Oosten M**, **Schäfer T**, **Gazendam JAC**, **et al**. Real-time in vivo imaging of invasive- and biomaterial-associated bacterial infections using fluorescently labelled vancomycin. *Nat Commun*. 2013;4(1):2584.
26. **Jie K**, **Deng P**, **Cao H**, **Feng W**, **Chen J**, **Zeng Y**. Prosthesis design of animal models of periprosthetic joint infection following total knee arthroplasty: A systematic review. *PLoS One*. 2019;14(10):e0223402.
27. **Tsang S-TJ**, **Morgan-Jones R**, **Simpson AHRW**. Debridement for prosthetic joint infections: future therapies. *Bone Joint Res*. 2020;9(6):311–313.
28. **Pijls BG**, **Sanders IMJG**, **Kuijper EJ**, **Nelissen RGHH**. Segmental induction heating of orthopaedic metal implants. *Bone Joint Res*. 2018;7(11):609–619.
29. **Sosa BR**, **Niu Y**, **Turajane K**, **et al**. 2020 John Charnley Award: The antimicrobial potential of bacteriophage-derived lysin in a murine debridement, antibiotics, and implant retention model of prosthetic joint infection. *Bone Joint J*. 2020;102-B(7_Supple_B):3–10.
30. **Pop TS**, **Zuh SG**, **Hidi M**, **Vass A**, **Gergely I**. IMPROVING QUALITY OF LIFE AFTER HIP REVISION ARTHROPLASTY. *European Scientific Journal, ESJ*. 2015;11:33.
31. **Antonios JK**, **Bozic KJ**, **Clarke HD**, **Spangehl MJ**, **Bingham JS**, **Schwartz AJ**. Cost-effectiveness of single vs double debridement and implant retention for acute periprosthetic joint infections in total knee arthroplasty: A Markov model. *Arthroplast Today*. 2021;11:187–195.
32. **Akram AR**, **Avlonitis N**, **Lilienkampf A**, **et al**. A labelled-ubiquicidin antimicrobial peptide for immediate *in situ* optical detection of live bacteria in human alveolar lung tissue. *Chem Sci*. 2015;6(12):6971–6979.
33. **Welling MM**, **Bunschoten A**, **Kuil J**, **et al**. Development of a hybrid tracer for SPECT and optical imaging of bacterial infections. *Bioconjug Chem*. 2015;26(5):839–849.
34. **Welling MM**, **Paulusma-Annema A**, **Balter HS**, **Pauwels EK**, **Nibbering PH**. Technetium-99m labelled antimicrobial peptides discriminate between bacterial infections and sterile inflammations. *Eur J Nucl Med*. 2000;27(3):292–301.
35. **Chen H**, **Liu C**, **Chen D**, **et al**. Bacteria-targeting conjugates based on antimicrobial peptide for bacteria diagnosis and therapy. *Mol Pharm*. 2015;12(7):2505–2516.
36. **Fleming GA**. Regulatory Considerations for Early Clinical Development of Drugs for Diabetes, Obesity, and Cardiometabolic Disorders. In: KrentzAJ, Heinemann L, Hompesch M, eds. *Translational Research Methods for Diabetes, Obesity and Cardiometabolic Drug Development: A Focus on Early Phase Clinical Studies*. London: Springer, 2015: 283–304.
37. **Kummar S**, **Doroshow JH**, **Tomaszewski JE**, **et al**. Phase 0 clinical trials: recommendations from the Task Force on Methodology for the Development of Innovative Cancer Therapies. *Eur J Cancer*. 2009;45(5):741–746.

Author information:
- M. M. Welling, PhD, Senior Postdoc
- K. Warbroek, BSc, Researcher
- C. Khurshid, PhD, Researcher
- M. N. van Oosterom, PhD, Postdoc
- F. W. B. van Leeuwen, PhD, Professor, Image-Guided Therapy, and Head of Interventional Molecular Imaging Laboratory
- T. Buckle, PhD, Assistant Professor
  Interventional Molecular Imaging Laboratory, Department of Radiology, Leiden University Medical Center, Leiden, Netherlands.
- D. D. D. Rietbergen, MD, PhD, Nuclear Medicine Physician, Interventional Molecular Imaging Laboratory, Department of Radiology, Leiden University Medical Center, Leiden, Netherlands; Department of Radiology, Section Nuclear Medicine, Leiden University Medical Center, Leiden, Netherlands.
- M. G. J. de Boer, MD, PhD, Medical Specialist Internal Medicine & Infectious Diseases, Departments of Internal Medicine and Infectious Diseases, Leiden University Medical Center, Leiden, Netherlands.
- R. G. H. H. Nelissen, MD, PhD, Professor of Orthopaedics and Chairman, Department of Orthopaedics
- B. G. Pijls, MD, PhD, Orthopedic Surgeon
  Department of Orthopedics, Leiden University Medical Center, Leiden, Netherlands.

Author contributions:
- M. M. Welling: Data curation, Formal analysis, Investigation, Methodology, Validation, Visualization, Writing – original draft, Writing – review & editing.
- K. Warbroek: Investigation, Methodology, Writing – review & editing.
- C. Khurshid: Investigation, Methodology, Writing – review & editing.
- M. N. van Oosterom: Investigation, Methodology, Software, Writing – review & editing.
- D. D. D. Rietbergen: Writing – review & editing.
- M. G. J. de Boer: Writing – review & editing.
- R. G. H. H. Nelissen: Writing – review & editing.
- F. W. B. van Leeuwen: Conceptualization, Funding acquisition, Methodology, Resources, Supervision, Validation, Writing – review & editing.
- B. G. Pijls: Funding acquisition, Investigation, Resources, Writing – review & editing.
- T. Buckle: Conceptualization, Investigation, Project administration, Supervision, Validation, Visualization, Writing – original draft, Writing – review & editing.

Funding statement:
- The authors disclose receipt of the following financial or material support for the research, authorship, and/or publication of this article: this research was funded by a NWO-TTW-VICI grant (TTW 16141) and a ZonMW-ENI-grant (09150161810084). KARL STORZ provided the prototype of the laparoscopic fluorescence camera.

ICMJE COI statement:
- B. G. Pijls reports collaboration with R. G. H. H. Nelissen as a co-inventor on a patent held by the Leiden University Medical Center (LUMC) (WO2020/067898), unrelated to this article.

Acknowledgements:
- We would like to thank Danny van Willigen for compound synthesis, and Romy van Leeuwerden, Imke Boekestijn, and Petra Dibbets for their assistance with the fluorescence and freehand SPECT (fhSPECT) imaging.

Open access funding
- The authors report that they received open access funding for their manuscript from a NWO-TTW-VICI grant (NWO TTW 16141).